

# 360-DEGREE VIDEO STITCHING FOR DUAL-FISHEYE LENS CAMERAS BASED ON RIGID MOVING LEAST SQUARES

Tuan Ho<sup>\*</sup>    Ioannis D. Schizas<sup>\*</sup>    K. R. Rao<sup>\*</sup>    Madhukar Budagavi<sup>†</sup>

<sup>\*</sup> Dept. of Electrical Engineering, University of Texas–Arlington, Arlington, TX USA

<sup>†</sup> Samsung Research America, Richardson, TX USA

## ABSTRACT

Dual-fisheye lens cameras are becoming popular for 360-degree video capture, especially for User-generated content (UGC), since they are affordable and portable. Images generated by the dual-fisheye cameras have limited overlap and hence require non-conventional stitching techniques to produce high-quality 360x180-degree panoramas. This paper introduces a novel method to align these images using interpolation grids based on rigid moving least squares. Furthermore, jitter is the critical issue arising when one applies the image-based stitching algorithms to video. It stems from the unconstrained movement of stitching boundary from one frame to another. Therefore, we also propose a new algorithm to maintain the temporal coherence of stitching boundary to provide jitter-free 360-degree videos. Results show that the method proposed in this paper can produce higher quality stitched images and videos than prior work.

**Index Terms**— 360-degree video, virtual reality, moving least squares, stitching, dual-fisheye

## 1. INTRODUCTION

Dual-fisheye lens cameras are becoming popular for 360-degree video capture, especially for UGC. Their portability and affordability give them an edge over traditional and professional 360-degree capturing systems such as [1][2] which usually deploy 6–17+ cameras on the same rig and are very expensive to own. An example dual-fisheye lens 360-degree camera is the Samsung Gear 360 which can produce 360x180-degree panoramas and video that are viewable on the 360-degree viewers such as Cardboard [3] or GearVR [4]. Other examples of dual-fisheye lens 360-degree cameras are Ricoh Theta [5] and LG 360 Cam [6] to name a few.

However, the convenience of a compact and affordable 360-degree capture system comes with a caveat. The images generated by the dual-fisheye lenses have limited overlap, and as we show in [7], the conventional stitching methods such as ones in [8] [9] do not provide satisfactory stitching results.

To stitch the images generated by the dual-fisheye lens cameras, [7] suggests a framework of four main stages, as shown in Figure 2(a). The first and second stages compensate

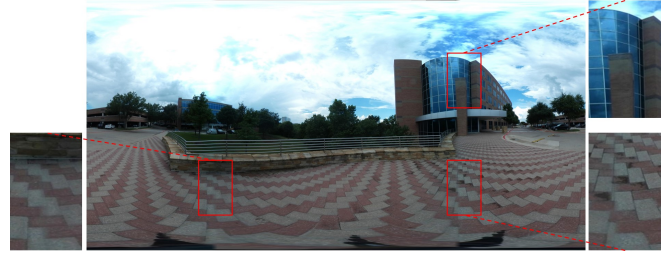


**Fig. 1.** 360x180-degree panorama stitched by [7] and the discontinuities in the overlapping regions.

for the light-fall off of the fisheye-lens camera and transform the light-compensated fisheye images into an equirectangular format that can be viewed on 360-degree players respectively. After the first two stages, the fisheye-unwarped images does not align with each other. Therefore, [7] proposes a two-step registration method that minimizes the discontinuity in the overlapping regions to align the images and blend them together. In this approach, the first step compensates for the geometric misalignment between the two fisheye lenses and depends on the camera parameters. The second step is a more refined alignment that adjusts any discontinuities caused by objects with varying depth in the stitching boundaries. In the first alignment, [7] solves an over-determined system for a warping matrix which is then used to align the images. This results in a least-squares approximated solution which globally transforms the images. Our observation is that typically the control points in the central part of the 360-degree image get aligned well resulting in improved quality compared to prior techniques. However, the control points at the top and bottom part of the image do not get aligned precisely leading to stitching artifacts in those regions. Figure 1 shows an example of visible discontinuities in the stitching boundary of pictures with patterns on the background.

This paper builds upon our previous work in [7] and improves the image alignment and stitching performance over the entire stitched 360x180-degree panoramas. It uses rigid moving least squares approach to achieve the improved alignment. This paper also extends the work to video stitching by incorporating a new temporal-coherent algorithm to produce jitter-free 360-degree videos.

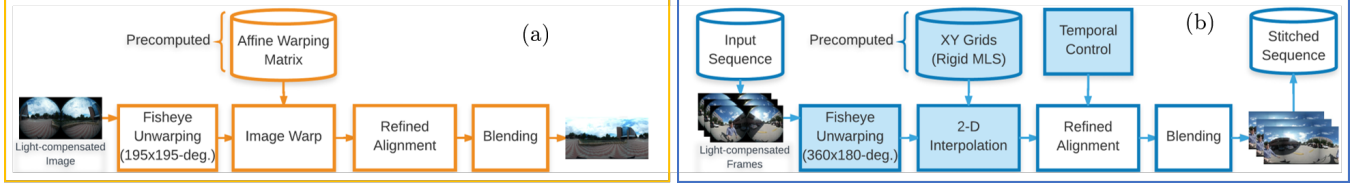


**Fig. 2.** The processing flow [7] (a) and the approach of this paper (b).

## 2. THE PROPOSED ALGORITHM

Figure 2(b) shows the block diagram of the proposed algorithm in this paper. Similar to [7], the proposed image alignment also has two steps – the first one is dependent on camera parameters, and the second step works adaptively to the scene. However, instead of estimating a warping matrix in a least-squares sense to align the pictures in the first step, we generate interpolation grids to deform the image based on rigid moving least squares (MLS) approach.

### 2.1. Rigid Moving Least Squares

Let  $p$  and  $q$  be the control points in the overlapping regions of the original and deformed images respectively. [10] defines three properties of an image deformation function  $f$  which are: interpolation ( $f(p_i) = q_i$  under deformation), smoothness (preserves smooth transition among pixels), and identity ( $q_i = p_i \Rightarrow f(v) = v$ ).

For every point in the image, we solve for a transformation matrix  $M$  that minimizes the weighted least squares:

$$\operatorname{argmin}_M \sum_i w_i \left\| \hat{p}_i M - \hat{q}_i \right\|^2 \quad (1)$$

where the weights  $w_i$  are proportional to the distance between the image point  $v$  and the control point  $p_i$  in the sense that  $w_i$  gets smaller when  $v$  moves further away from  $p_i$  (i.e. the least squares minimization depends on the point of evaluation, thus the name moving least squares). When  $v \rightarrow p_i$ ,  $f$  interpolates  $f(v) = q_i$ . [10] defines such weights as:

$$w_i = \frac{1}{|p_i - v|^{2\alpha}}$$

$\hat{p}_i = v - p^*$  and  $\hat{q}_i = q^*$  are derived from each point  $v$  in the image and the weighted centroids  $p^*$  and  $q^*$  [10].

For control points selection, we adopted the checkerboard experiment from [7] with our method of picking the correspondence points. In this experiment, both fisheye lenses, each has 195-degree field of view, see the same checkerboards on their sides. The images taken by the fisheye lenses are unwrapped to 360x180-degree equirectangular planes. We then arrange the unwrapped images so that the right image is positioned at the center of the 360x180-degree plane, while the left image is split and put to the sides of the plane. With this

arrangement, the overlapping regions are ready for control-point selection. By choosing the same checkerboards' cross sections on the unwrapped images, one can visualize the geometric misalignment between the two lenses. Figure 3 shows the selected control points  $\{p\}_i$  and  $\{q\}_i$ , which indicate the differentiated positions of the same points in the stitching boundaries of the two images. Our interest is to determine the function  $f_r$  that does the transformation  $f_r(p_i) = q_i$  in the overlapping regions while keeping the other areas of the image as visually intact as possible.

While the MLS is general in the matrix  $M$  in (1), we are only interested in the rigid transformation since it generates more realistic results than affine and similarity transformations. The similarity transformations are a subset of the affine transformations that have only translation, rotation, and uniform scaling. The similarity matrix  $M$  is defined such that  $M^T M = \lambda^2 I$  (e.g. a rotation matrix).  $\lambda^2$  acts as a uniform scaling factor. In rigid transformation, it is desirable that no uniform scaling is included. [10] proposed a theorem that relates the MLS solution for  $M^T M = \lambda^2 I$  (similarity transformation) to its solution of  $M^T M = I$  (rigid transformation), and derived the solution for the rigid MLS function  $f_r$ . We invite readers to read [10] for more details about the mathematical treatment used here.

We generate the rigid-MLS interpolation grids to deform the right unwrapped image (i.e. to apply  $f_r$  over the image), thus aligning it with the left one. Figure 4 shows the right unwrapped fisheye image gets deformed by the rigid MLS method. While the portions of the image in proximity to the stitching boundaries are transformed to match the other image, the remaining of the deformed picture have no discernible difference compared to the original.

### 2.2. Refined Alignment

The rigid MLS aligns the control points around the stitching boundary, thus registering the two unwrapped fisheye images together. However, when the depth of the object in the overlapping areas changes, it introduces misalignment to the scene. Therefore, a refined alignment is necessary after the rigid MLS deformation. To this end, we adopt the same adaptive method of using the normalized cross-correlation matching in [7] to further align the images.

The refined alignment performs a fast template matching and utilizes the matching displacements on both stitching

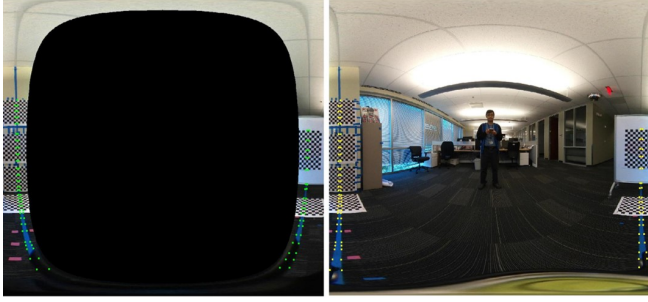


**Fig. 3.** Left: the overlapping areas on the unwarped left image and  $\{q\}_i$  (green dots). Right: unwarped right image and  $\{p\}_i$  (yellow dots).



**Fig. 4.** The original and the rigid-MLS-deformed images with their control points  $\{p\}_i$  and  $\{q\}_i$  overlayed.

boundaries to generate eight pairs of control points. These points are then used to solve for a 3x3 affine matrix to warp the deformed image. As a least-squares solution, this refined method is not sufficient in registering images with complicated misalignment patterns, but it works very well for those with minor misalignment such as the one caused by the varied object's depth. Figure 5 shows that the refined alignment minimizes the discontinuity when the person is sitting close to the camera's stitching boundary.

### 3. EXTENSION TO 360-DEGREE VIDEO

In the 360-degree video stitching, it is essential to minimize jitters—the abrupt transition between the stitched frames so that the final video appears continuous and comfortable to view. Adjacent frames in the sequence that are not stitched by the same measure can generate jitters. In the work presented here, when a bad match occurs without getting filtered out in the refined alignment, it generates a false warping matrix that abruptly distorts the stitching boundary of the picture. This attenuated scene causes jitter which is the result of the sudden transition between the previous well-stitched frame and the current bad-stitched one. Therefore, it is important to guarantee good matches throughout the entire sequence to maintain smooth frame-to-frame transition, and thus minimize jitters.

Algorithm 1 illustrates our method to maintain the tem-

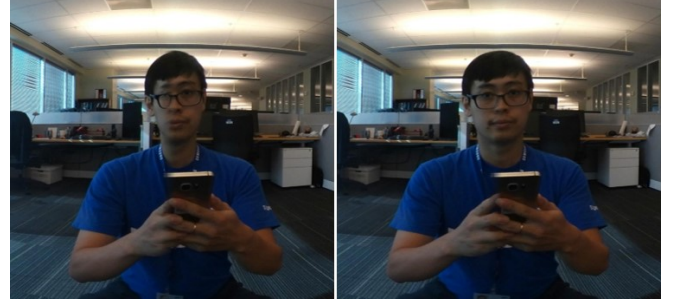


**Fig. 5.** The person sitting close to the camera and in the stitching boundary. Left: after rigid MLS deformation. Right: after rigid MLS deformation and refined alignment.

---

#### Algorithm 1: Refined Alignment (with jitter control)

---

**Input:** *leftImage*, *rightImage* (deformed)

```

1 (scoreLeft, scoreRight) ← TemplMatch();
2 if ( both matching scores are good ) then
3   Estimate affine warping matrix affineMat;
4   Store affineMat for the next frame;
5   warpEn ← 1;
6 else // bad scores on either boundary
7   if matching scores of the previous frame are good
8     then
9       warpEn ← 1;
10      affineMat ← previous affineMat;
11   else
12     warpEn ← 0; // don't warp image
13   end
14 if ( warpEn ) then
15   Warp rightImage by affineMat;
16 end

```

---

poral coherence for the sequence. A good score is returned at one stitching boundary if all of the followings satisfied. First, the peak normalized cross-correlation is larger than 0.85/1.0. Second, the returned vertical displacement is in the margin of  $[-10, +10]$  pixels. Third, the horizontal displacement of the current match must not exceed 10% margin compared to its of the previous frame. These constraints, obtained from our empirical experiments, are set to eliminate bad matching caused by poor lighting and abrupt movements of the boundaries in horizontal and vertical directions.

### 4. IMPLEMENTATION AND RESULTS

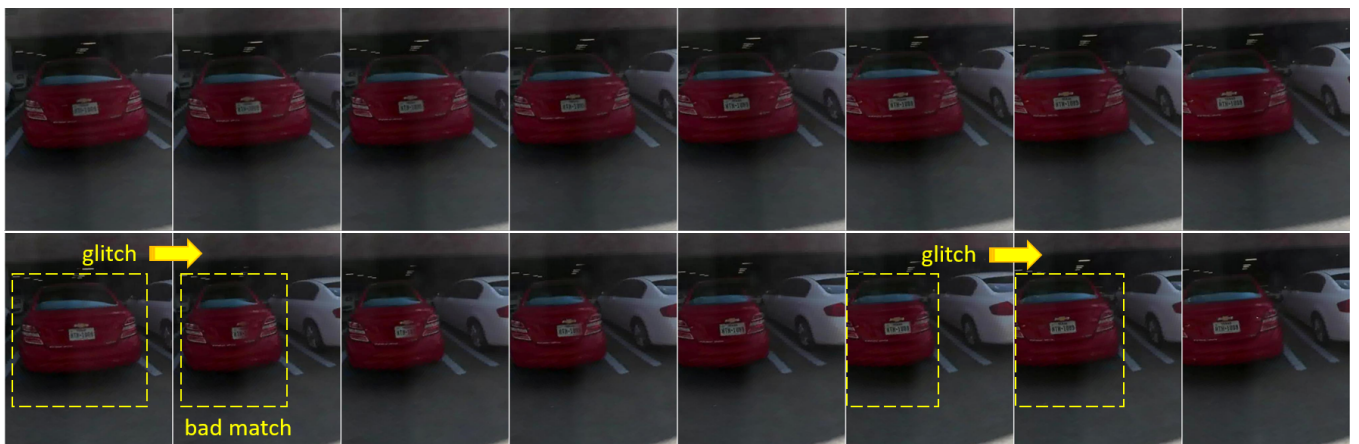
We have implemented the proposal algorithm in C++ and Matlab. The rigid MLS grids are precomputed, and the deformation becomes an interpolation process that can be accelerated by GPU.

Figure 6(a) illustrates an image stitched by the proposed





**Fig. 6.** (a) 360x180-degree panorama stitched by this proposal. (b)(c) The stitching boundaries in (a) (top row) compared to the same image stitched by [7] (bottom row).



**Fig. 7.** Stitching boundary in consecutive frames. Stitched by the proposal (top row), and by [7] (bottom row).

method. In this picture, there are a fence, buildings, and patterned background on the stitching boundaries. Figure 6(b) shows the comparison of the stitching boundaries in the image stitched by the proposal and by [7] (also in Figure 1). While the discontinuities appear in the stitching boundaries in [7] as the result of the least-squares solution, the proposed method produces seamless 360-degree panorama thanks to the rigid MLS deformation.

For video stitching<sup>1</sup>, Figure 7 demonstrates the adjacent stitched frames created by the proposal (top row, no jitter) and by [7] (bottom row). In the bottom row, the first jitter occurs when the refined alignment lets a bad match get through, resulting in an affine transformation that moves the image on the right side of the stitching boundary to the left. As a result, the car in the boundary gets distorted leading to an abrupt transition between the frames.

<sup>1</sup>This paper has supplementary downloadable materials, which are the stitched videos generated by this novel method and by [7].

## 5. CONCLUSION

This paper has introduced a novel method for stitching the images and video sequences generated by the dual-fisheye lens cameras. The proposed alignment has two steps. The first one, carried out offline, compensates for the sophisticated geometric misalignment between the two fisheye lenses on the camera based on rigid moving least squares approach. The second step, applied online and adaptively to the scene, provides a more refined adjustment for any misalignment created by the objects with varying depth on the stitching boundaries. We extend the proposed approach to 360-degree video stitching with the relevant constraints to maintain the smooth transition between frames and therefore minimize jitters. Results show that our method not only generates more accurately stitched 360x180-degree images but also jitter-free 360-degree videos.

## 6. REFERENCES

- [1] “GoPro Odyssey,” <https://gopro.com/odyssey>, [Retrieved August, 2016].
- [2] “Facebook Surround360,” <https://facebook360.fb.com/facebook-surround-360>, [Retrieved August, 2016].
- [3] “Google Cardboard,” <https://vr.google.com/cardboard>, [Retrieved August, 2016].
- [4] “Samsung GearVR,” [www.samsung.com/us/gearvr](http://www.samsung.com/us/gearvr), [Retrieved August, 2016].
- [5] “Ricoh Theta,” <https://theta360.com>, [Retrieved August, 2016].
- [6] “LG 360 Cam,” <http://www.lg.com/us/mobile-accessories/lg-LGR105-AVRZTS-360-cam>, [Retrieved August, 2016].
- [7] T. Ho and M. Budagavi, “Dual-fisheye lens stitching for 360-degree imaging,” in *Proc. of the 42nd IEEE International Conference on Acoustics, Speech and Signal Processing (ICASSP’17)*, 2017 (Accepted).
- [8] M. Brown and D.G. Lowe, “Automatic panoramic image stitching using invariant features,” *International Journal of Computer Vision*, vol. 74, pp. 59–73, August 2007.
- [9] R. Szeliski, *Computer Vision: Algorithms and Applications*, Springer, London, UK, 1st edition, 2011.
- [10] S. Schaefer, T. McPhail, and J. Warren, “Image deformation using moving least squares,” in *Proc. of ACM SIGGRAPH ’06*, 2006.